Synthesis of hybrid nanocomposites by sol-gel method and their characterizations

N. Ben Mansour[a], G. Khouqeer[b], N. Abdel All[b,c], J. El Ghoul[a,b,*]
[a]*Laboratory of Physics of Materials and Nanomaterials Applied at Environment (LaPhyMNE), Gabes University, Faculty of Sciences in Gabes, 6072, Tunisia*
[b]*Department of Physics, College of Sciences, Imam Mohammad Ibn Saud Islamic University (IMSIU), Riyadh 11623, Saudi Arabia*
[c]*Physics Department, Assiut University, Assiut 71516, Egypt*

In this work, we report the synthesis of different hybrid nanocomposites by sol-gel method. Therefore, we used picric acid as a catalyst to incorporate the nanopowder oxides of nickel (NiO), copper (CuO) and manganese (MnO) in the porous carbon matrix based on pyrogallol and formaldehyde (PF). After a drying and heat treatment for two hours at 650 °C pyrolysis temperature, the obtained materials have been characterized by different structural and electrical techniques. The X-ray diffraction (XRD) spectra show that the incorporation of inorganic nanoparticles improved the crystallization of different nanocomposites with the existance of a graphite phase. The transmission electron microscopy (TEM) images reveal that the graphite nanoparticles size depends to the incorporated inorganic oxide. From the electrical studies, we notice that electrical conduction is linked to the presence of graphite nanoparticles. The variation of the electrical conductivity and the relaxation time with the measurement temperature, ranging between 80 and 300 K, explain the effect of the hopping conduction mechanism in these nanocomposites.

(Received October 12, 2021; Accepted January 28, 2022)

Keywords: Carbon matrix, Inorganic nanopowders, Nanocomposite, Electrical conductivity, Hopping conduction mechanism

1. Introduction

The porous carbon matrix has been widely applied to develop promising materials in a variety of fields, including greenhouse gas adsorption and separation [1,2]. This matrix does, in fact, have a unique pore structure, as well as good stability and minimal preparation costs [3,4]. One of the organic gels known for its promising potential features depending on the synthesis condition is the porous carbon matrix based on pyrogallol-formaldehyde (PF) [5]. The implantation of inorganic nanoparticles in a porous carbon matrix leads to the formation of various hybrid organic/inorganic nanocomposites [6-8]. Researchers have paid a lot of attention to these hybrid nanocomposites in recent years, whether from an applied or basic standpoint [9,10]. They're extensively applied in a variety of applications, including photovoltaic cells [11], hydrogen storage [12], negatronic devices [13] and electrochemical devices such as sensors [14]. In fact, the inorganic nanoparticles are scientifically and technologically interesting functional materials with a variety of properties spanning nearly all aspects of materials science and physics. They are very important for research because of their importance in applications in biology, environment, analytical chemistry and physics [15]. In fact, these nanoparticles characterized by a high surface/volume ratio, low toxicity, high chemical stability, and quick electron transfer capabilities, which improve the performance of nanomaterials when applied as biomimetic membranes to detect proteins and maintain their activity [16,17]. Nevertheless, the incorporation of inorganic nanoparticles into a porous carbon matrix has led the way for a new class of materials with unique electrical and optical properties, making them appealing for use in disciplines such as optoelectronics [18], sensor design [19,20], and catalysis [21]. The interfacial interplay between

* Corresponding author: jmalghoul@imamu.edu.sa
https://doi.org/10.15251/JOR.2022.181.57

the inorganic nanoparticles and the PF porous matrix is crucial in determining the hybrid nanocomposites' various electrical characteristics. The establishment of unique interface regions between carbon matrix and inorganic nanoparticles has been widely attributed to the origin of electrical transport phenomena. Interfaces play a critical role in improving conductivity and other electrical properties of these nanocomposites. Therefore, the synthesis, characterization, and understanding of the electrical conduction process in these materials are the main goals of this research.

2. Experimental procedure

2.1. Preparation

The synthesis of PF porous carbon matrix and PF/NiO, PF/CuO and PF/MnO nanocomposites has been carried by sol-gel method. Firstly, each of precursors of nickel (II) chlorid (NiCl2,6H2O), copper (II) acetylacetonate (C10H14CuO4) and manganese (II) chlorid tetrahydrate (MnCl2,4H2O) was dissolved in methanol. After 15 min under magnetic stirring at room temperature, the solutions were then placed in an autoclave and dried in supercritical conditions of ethyl alcohol. The obtained nanopowders were annealed at 500 °C in air for two hours and mixed with mass proportion of 5% in pyrogallol (P), formaldehyde (F) and water solution. Then, we used the picric acid for the reaction activation. Secondly, the drying of the obtained wet gel was carried at 50 °C during 15 days. In the goal to avoid any shrinkage of the xerogel monolith obtained, the wet gel undergoes a drying with heating rate of 10 ° C./day up to 150 ° C.

Finally, the different nanocomposites were obtained after a conventional drying like that of the PF matrix. In our case, the heat treatment of all samples was carried at 650 °C with a heating rate of 5 °C/min in a tubular furnace under controlled nitrogen atmosphere during two hours. After natural cooling, we prepared the samples in a parallelepipedal form (12x6x3) mm3 with an ohmic contact in silver paint on two parallel faces for the electrical measurements.

2.2. Characterization

The obtained samples were studied by by XRD from a Bruker X-ray diffractometer D5005 with CoKα radiation. For the morphological study, we use a JEOL-100C TEM. An Agilent-4294A impedance analyzer with an excitation voltage of 50 mV was used for measurements of electrical conductivity and relaxation time for frequencies ranging from 40 Hz to 10 MHz. The variation of measurement temperature was provided by a VPF-100 cryostat cooled with liquid nitrogen from Janis Corporation.

3. Results and discussions

Figure 1 shows the XRD patterns of the resulting PF matrix and various nanocomposites. In the PF matrix, two large diffraction peaks at at 24° and 42° were found, attributable to the (002) and (100) planes typical of amorphous carbon. The diverse nanocomposites, on the other hand, have crystallized. Clear that, there are three distinct metallic nickel reflection peaks appear in PF/NiO nanocomposite, three distinct metallic copper reflection peaks in PF/CuO nanocomposite, and two phases of manganese oxide MnO and metallic manganese Mn appear in PF/MnO nanocomposite. Scherrer's formula Eq. (1) was used to calculate the crystallite size of the PF matrix and other nanocomposites [23]:

$$G = \frac{0.9\lambda}{B\cos\theta_B} \tag{1}$$

where θ_B is the maximum Bragg diffraction peak and *B* is the line width at half maximum and λ is the X-ray wavelength. The average value of graphite crystallites was determined to be around 2 nm for the PF matrix, 3.5 nm, 5 nm, and 15 nm for the PF/NiO, PF/CuO, and PF/MnO nanocomposites, respectively, according to the dimension of the crystallites deduced using Eq. (1). The average size of the other types of crystallites (Ni, Cu, Mn, and MnO) varies between 12 nm and 50 nm. According to these results deduced that, the integration of inorganic nanoparticles into the carbon matrix under the influence of pyrolysis temperatures of 650 °C leads to a change in the crystalline characteristics of distinct nanocomposites compared to those of the PF matrix.

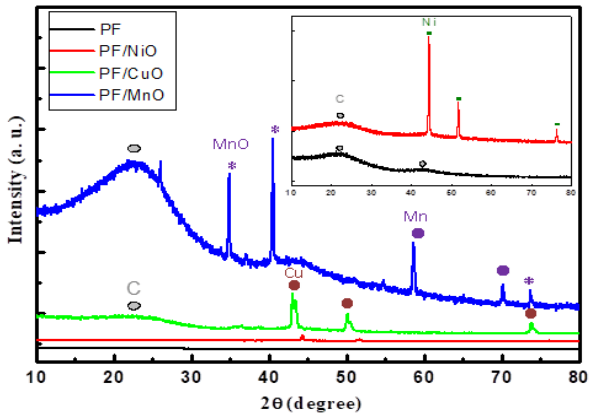

Fig. 1. XRD patterns of the all prepared samples.

Figure 2 illustrates the TEM observations for the samples under consideration. The size of the nanoparticles varied with the integrated oxide, as shown in these images. It noticed that the nanoparticles in all samples have agglomerated together. The PF organic matrix yielded the smallest size, while the PF/MnO nanocomposite produced the largest. These micrographs match the XRD results.

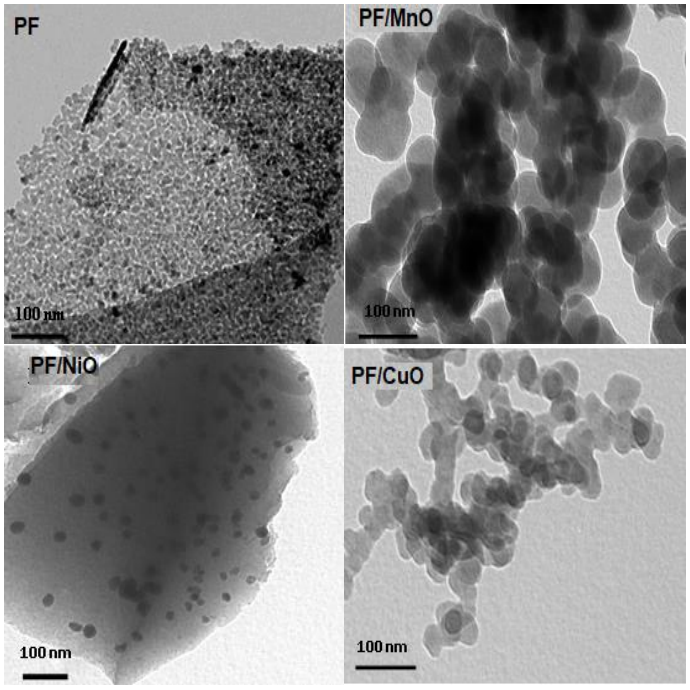

Fig. 2. TEM micrographs of the different prepared samples.

The electrical conductivity of the investigated material was determined using Eq. (2) according to the value of the resistance R obtained by the impedance analyzer at low frequency.

$$\sigma = L/RS \tag{2}$$

where L is the pellet's thickness and S is the electrode's contact area. The presence of a linear form in the change of electrical conductivity versus T-1/4 (Fig. 3) indicates that the 3D Godet-Variable Range Hopping (3D-GVRH) mechanism may be appropriate to characterize the temperature dependence of conductivity [24].

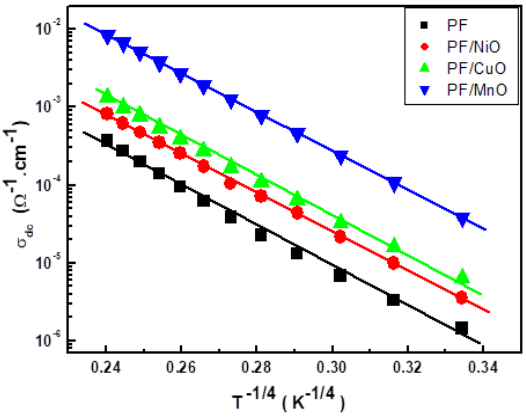

Fig. 3. Variation of the dc conductivity versus $T^{-1/4}$.

When the charge carrier interaction is ignored in this model, the dc conductivity is given by Eq. (3):

$$\sigma_{dc} = \sigma_0 \exp\left(-\frac{T_0}{T}\right)^{1/4} \tag{3}$$

where σ_0 is a pre-exponential factor, T is the measurement temperature. T_0 is the Godet characteristic temperature, which is calculated using Eq. (4) [25]:

$$T_0 \cong 310\frac{\alpha^3}{N(E_F)k_B} \tag{4}$$

where $N(E_F)$ is the density of states, k_B is the constant of Boltzmann and $1/\alpha$ is the carrier localization length.

The variability in electrical conductivity and density of states for the different samples at room measurement temperature is shown in Fig. 4. From those two curves, the density of states and electrical conductivity are inversely correlated. Indeed, with minimum conductivity, N(Ef) achieves the greatest value in the PF matrix. N(Ef) tends to a minimal value with a maximum conductivity in the PF/MnO nanocomposite. This proves that the formation of the states responsible for charge transport is not the source of electrical conductivity.

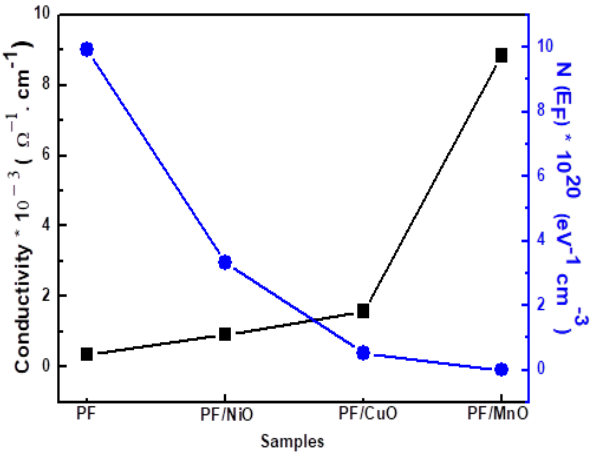

Fig. 4. Electrical conductivity and density of states for the all samples.

We have shown the variation of electrical conductivity and the size of graphite crystallites for different samples in Fig.5 to determine the origin of the increase in its electrical conductivity. According to the two curves, the electrical conductivity and the size of graphite crystallites are proportional. This proves that the size of graphite nanoparticles is the source of electrical conductivity.

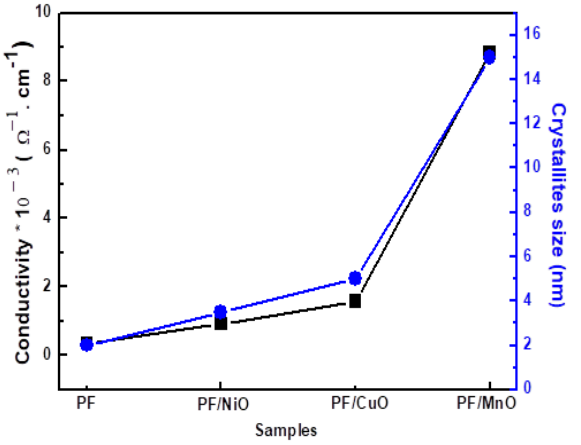

Fig. 5. Electrical conductivity and crystallites size of graphite for the different samples.

In Fig. 6, the electrical conductivity vs 1000/T is plotted on a semi-log scale. The electrical conductivity of our samples increases as the measurement temperature increases, proves their semiconductor behavior characteristics. According to Eq. (5), the curves show activation temperature dependence [26]:

$$\sigma = A\exp\left(-\frac{E_a}{k_B T}\right) \tag{5}$$

where activation energy, E_a and A is the pre-exponential factor. According to Eq. (5), the activation energies estimated from the linear fit at high temperature for PF, PF/NiO, PF/CuO, and PF/MnO samples are 101, 92, 90, and 81 meV, respectively. The integration of inorganic

nanoparticles in the carbon matrix PF decreased the graphite inter-particles distance and favorably increased electrical conductivity in our samples, resulting in lower activation energy values.

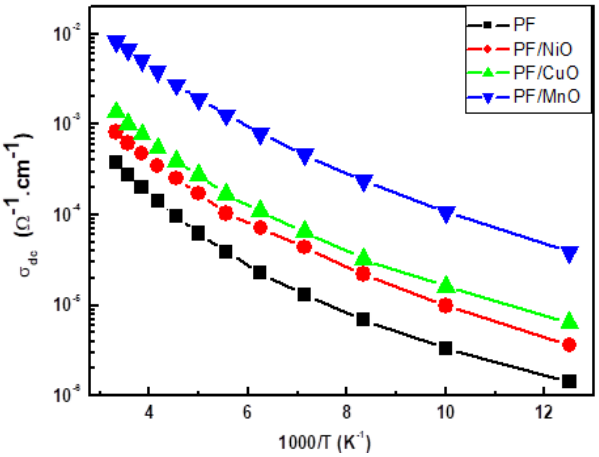

Fig. 6. Variation of the dc conductivity versus 1000/T.

The impedance measurements were done at frequencies ranging from 40 Hz to 100 MHz. We estimated the relaxation time for measurement temperatures between 80 and 300 K using the variation of the imaginary part of the impedance as a function of frequency.

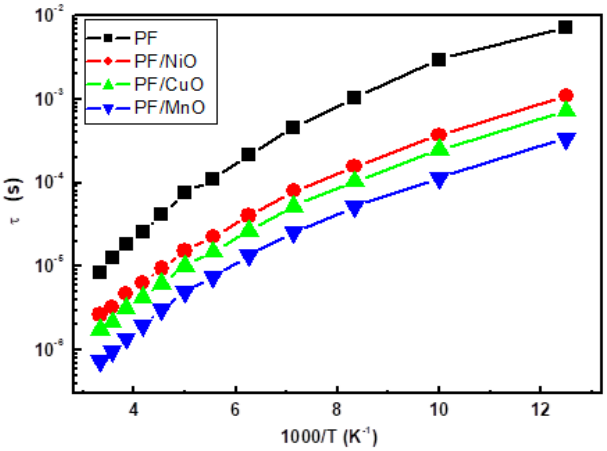

Fig. 7. Variation of the relaxation time versus 1000/T.

The variance of the relaxation time as a function of the inverse of measurement temperature is shown in Fig. 7. According to Eq. (6), the curves show activation temperature dependence.

$$\tau = \tau_0 \exp\left(\frac{E_a'}{k_B T}\right) \tag{6}$$

where τ_0 is the pre-exponential factor and E_a' is the activation energy of relaxation time. According to Eq. (6), the values of Ea' for PF, PF/NiO, PF/CuO, and PF/MnO samples are 104, 94, 93, and 84 meV, respectively. These values agree well with those derived from electrical conductivity, confirming that the hopping conduction mechanism dominates in both dc and ac modes.

Fig. 8 shows the variation of electrical conductivity versus the relaxation time in log-log scale. The measured linearity confirms that conductivity is related to relaxation time for the various samples investigated. This proportionality could be seen in materials characterized with hopping charge transport [27,28].

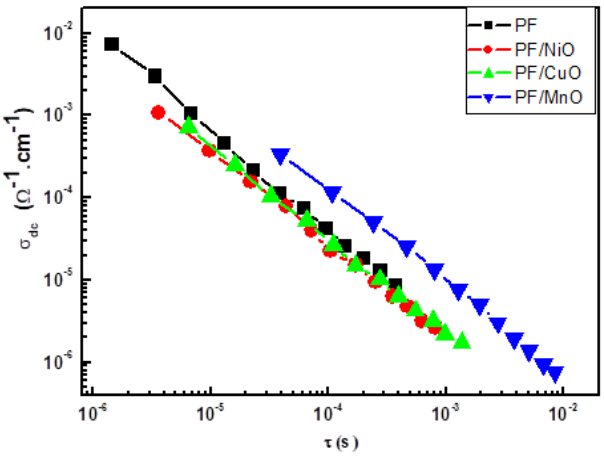

Fig. 8. Variation of dc conductivity versus the relaxation time.

4. Conclusion

The effects of NiO, CuO, and MnO nanoparticles on the structural, morphological, and electrical properties of a porous carbon matrix based on pyrogallol-formaldehyde synthesized by the sol-gel method was studied. The structural and morphological characterizations show that the nanoparticle size varies depending on the incorporating metallic oxide. The size of graphite nanoparticles explains the change in conductivity as a function of the inserted metallic oxide. In both the dc and ac regimes, the hopping conduction mechanism dominates.

Acknowledgments

The authors extend their appreciation to the Deanship of Scientific Research at Imam Mohammad Ibn Saud Islamic University for funding this work through Research Group no. RG-21-09-41.

References

[1] D. Jayne, Y. Zhang, S. Haji, C. Erkey, Dynamics of removal of organosulfur compounds from diesel by adsorption on carbon aerogels for fuel cell applications. Int. J. Hydrogen Energy 2005, 30, 1287. ; https://doi.org/10.1016/j.ijhydene.2005.03.014

[2] K.Y. Kang, B.I. Lee, J.S. Lee, Hydrogen adsorption on nitrogen doped carbon xerogels. Carbon 2009, 47, 1171 ; https://doi.org/10.1016/j.carbon.2009.01.001

[3] K.P. Wang, H. Teng, The performance of electric double layer capacitors using particulate porous carbons derived from PAN fiber and phenol-formaldehyde resin. Carbon 2006, 44, 3218. ; https://doi.org/10.1016/j.carbon.2006.06.031

[4] F.J. Maldonado-Hodar, C. Moreno-castilla, A.F. Perez-Dadenas, Surface morphology, metal dispersion, and pore texture of transition metal-doped monolithic carbon aerogels and steam-activated derivatives. Microporous Mesoporous Mater 2004, 69, 119. ; https://doi.org/10.1016/j.micromeso.2004.02.001

[5] L. El Mir, S. Kraiem, M. Bengagi, E. Elaloui, A. Ouderni, S. Alaya, Synthesis and

characterization of electrical conducting nanoporous carbon structures. Physica B 2007, 395, 104 ; https://doi.org/10.1016/j.physb.2007.02.068

[6] N. Ben Mansour, L. El Mir, Study of carbon/copper nanocomposite synthesized by sol-gel method. Journal of Materials Science: Materials in Electronics 2016, 27, 11682 ; https://doi.org/10.1007/s10854-016-5304-9

[7] N. Ben Mansour, L. El Mir, Influence of the nickel oxide nanoparticles content on the electrical properties of carbon/nickel nanocomposites. Journal of Materials Science: Materials in Electronics 2017, 28, 11284 ; https://doi.org/10.1007/s10854-017-6919-1

[8] N. Ben Mansour, L. El Mir, Origin of dc and ac electric transport phenomena in carbon/manganese oxide nanocomposite. Journal of Solid State Sciences 2018, 85, 38 ; https://doi.org/10.1016/j.solidstatesciences.2018.09.010

[9] A. Okada, A. Usuki. The chemistry of polymer-clay hybrids. Mater. Sci. Eng. 1995, 3,109 ; https://doi.org/10.1016/0928-4931(95)00110-7

[10] E.P. Giannelis, Polymer Layered Silicate Nanocomposites. Adv. Mater. 1996, 8, 29 ; https://doi.org/10.1002/adma.19960080104

[11] W.J.E. Beek, M.M. Wienk, M. Kemerink, X. Yang, R.A.J. Janssen. Hybrid Zinc Oxide Conjugated Polymer Bulk Heterojunction Solar Cells. J. Phys. Chem. B 2005, 109, 9505 ; https://doi.org/10.1021/jp050745x

[12] S.F. Wang, F. Xie, R.F. Hu, Sens. Carbon-coated nickel magnetic nanoparticles modified electrodes as a sensor for determination of acetaminophen. Actuators B 2007, 123, 495 ; https://doi.org/10.1016/j.snb.2006.09.031

[13] N.A. Filinyuk, Proceedings of a USSR Scientific and Technical Conference on Devices with Negative Resistance and Integrated Converters on Their Basis, Baku, Russian 1991, 11.

[14] M. Zielinski, R. Wojcieszak, S. Monteverdi, M. Mercy, M.M. Bettahar, Hydrogen storage in nickel catalysts supported on activated carbon. Int. J. Hydrogen Energy 2007, 32, 1024 ; https://doi.org/10.1016/j.ijhydene.2006.07.004

[15] G. Malandrino, S.T. Finocchiaro, R.T. Nigro. Free-Standing Copper(II) Oxide Nanotube Arrays through an MOCVD Template Process. Chem. Mater. 16 (2004) 5559 ; https://doi.org/10.1021/cm048685f

[16] N. Chopra, V.G. Gavalas, L.G. Bachas, B.J. Hinds, L.G. Bachas, Functional one-dimensional nanomaterials: applications in nanoscale biosensors. Anal. Lett. 2007, 40, 2067 ; https://doi.org/10.1080/00032710701567170

[17] K. Kerman, M. Saito, S. Yamamura, Y. Takamura, E. Tamiya, Nanomaterial-based electrochemical biosensors for medical applications. Trends Anal. Chem. 2008, 27, 585 ; https://doi.org/10.1016/j.trac.2008.05.004

[18] R.C. Jin, Y.W. Cao, C.A. Mirkin, K.L. Kelley, G.C. Schatz, J.G. Zheng, Photoinduced Conversion of Silver Nanospheres to Nanoprisms. Science 2001, 294, 1901 ; https://doi.org/10.1126/science.1066541

[19] M. Hjiri, R. Dahari, N. Ben Mansour, L. El Mir, M. Bonyani, A. Mirzaei, S.G. Leonardi, G. Neri, Electrochemical properties of a novel Ni-doped nanoporous carbon. Materials Letters 2015, 160, 452 ; https://doi.org/10.1016/j.matlet.2015.08.001

[20] S. Marini, N. Ben Mansour, M. Hjiri, R. Dhahri, L. El Mir, C. Espro, A. Bonavita, S. Galvagno, G. Neri, S.G. Leonardi, Non-enzymatic Glucose Sensor Based on Nickel/Carbon Composite. Electroanalysis 2018, 30, 1 ; https://doi.org/10.1002/elan.201700687

[21] D.M. Vriezema, M.C. Aragones, J.A.A.W. Elemans, J.J.L.M. Cornelissen, A.E. Rowan, R.J.M. Nolte, Self-Assembled Nanoreactors. Chem. Rev. 2005, 105, 1445 ; https://doi.org/10.1021/cr0300688

[22] L. El Mir, A. Amlouk, C. Barthou, S. Alaya, Synthesis and luminescence properties of ZnO/Zn 2SiO 4/SiO 2 composite based on nanosized zinc oxide-confined silica aerogels. Physica B: Condensed Matter 2007, 388. 412 ; https://doi.org/10.1016/j.physb.2006.06.151

[23] H. Saeki, H. Tabata, T. Kawai, Magnetic and electric properties of vanadium doped ZnO

films. Solid State Commun. 2001, 120, 439 ; https://doi.org/10.1016/S0038-1098(01)00400-8

[24] C. Godet, Variable range hopping revisited: the case of an exponential distribution of localized states. J. Non-Cryst. Solids, 2002, 299, 333 ; https://doi.org/10.1016/S0022-3093(01)01008-0

[25] C. Godet, Electronic localization and bandtail hopping charge transport. Phys. Stat. Solidi B, 2002, 231, 499 ; https://doi.org/10.1002/1521-3951(200206)231:2<499::AID-PSSB499>3.0.CO;2-K

[26] N.F. Mott, E.A. Davis, Electronic Processes in Non-Crystalline Materials, Clarendon, Oxford 1979, 157.

[27] J.C. Dyre, The random free- energy barrier model for ac conduction in disordered solids. J. Appl. Phys. 1988, 64, 2456 ; https://doi.org/10.1063/1.341681

[28] H. Jhans, D. Kim, R.J. Rasmussen and J.M. Honig, ac-conductivity measurements on La2NiO4+δ. Physical review B 1996, 54, 16. https://doi.org/10.1103/PhysRevB.54.11224